Supplementary Information (SI) for Journal of Materials Chemistry A.

Supporting Information for

Significantly Enhanced Properties of Micro-ionic Thermocells through Microstructure Interfacial Effect

Hongwei Chen, Shuqi Zhao, Haoyu Zou, Ming Qu, Fanghao Zhong, Xiang Wei, Yangfan Song, and Zhuo Liu[*]

Hebei Key Laboratory of Low Carbon and High Efficiency Power Generation Technology, North China Electric Power University, Baoding, Hebei Province 071003, China.

* Corresponding author: Zhuo Liu, Email: zhuoliu@ncepu.edu.cn

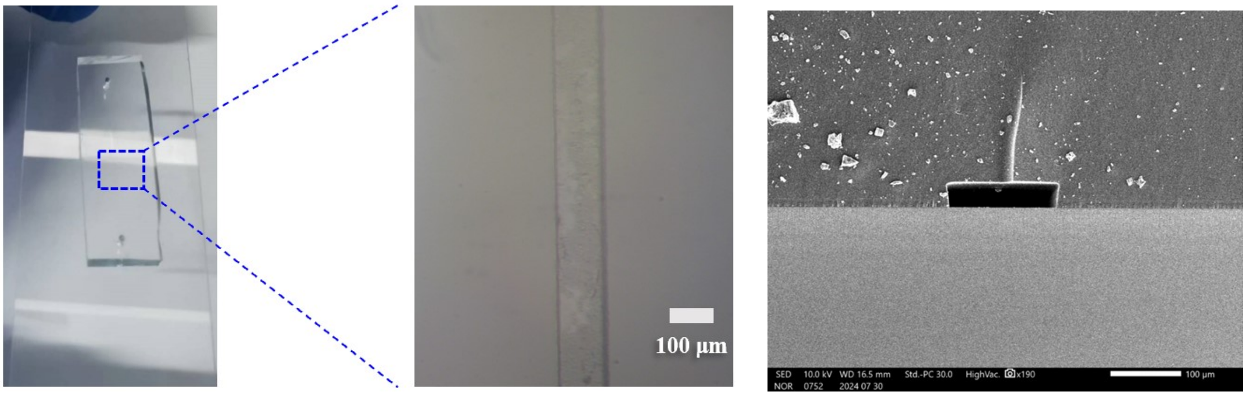

Scheme S1 Images and morphology of the microstructure of MiTCs during optical microscope and SEM.

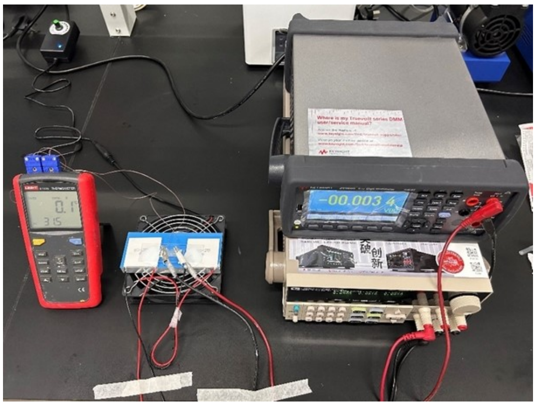

Scheme S2 Images of the home-made testing system for MiTCs

The ionic thermoelectric properties of pure redox electrolytes were calibrated by a home-made straight system as shown in Scheme S3. The home-made straight system can measure the intrinsic thermoelectric properties of electrolytes and was used for comparison with that in MiTCs. The results were consistent with that reported in literatures[1], confirming its feasibility for ionic thermoelectric properties of redox electrolytes.

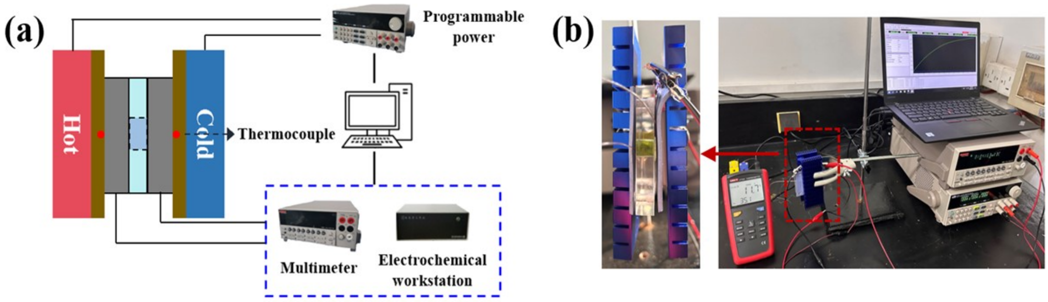

Scheme S3 Schematic diagram of the home-made straight system for redox electrolytes calibration

Preparation of the $K_3Fe(CN)_6$/$K_4Fe(CN)_6$ electrolytes: A mixed $K_3Fe(CN)_6$/$K_4Fe(CN)_6$ electrolytes (0.05~0.4 mol L^{-1}) was prepared by dissolving a certain mass of potassium ferricyanide ($K_3Fe(CN)_6$) and potassium ferrocyanide trihydrate ($K_4Fe(CN)_6$) in deionized (DI) water with stirring for 30 min for experiments. In all the experiments, the concentration of $K_3Fe(CN)_6$ and $K_4Fe(CN)_6$ are equimolar, and their maximum solubility is ca. 0.4 mol L^{-1} in DI water, which is consistent with that in literature[1]. In addition, KCl were used as THE supporting electrolytes, and added into the $K_3Fe(CN)_6$/$K_4Fe(CN)_6$ electrolytes with stirring for 30 min.

Ionic thermoelectric properties: The ionic thermoelectric properties of MiTCs include the ionic thermopower, ionic conductivity and normalized maximum power density ($P_{max}/\Delta T^2$). In terms of the ionic thermopower of MiTCs, the open-circuit voltages between the two electrodes were recorded at different temperature gradients by using a Keithley 2000E source/meter. The ionic thermopower (S_i) can be calculated as follows:

$$S_i = \frac{\Delta U}{\Delta T}\frac{d_2}{d_1} \tag{1}$$

Where ΔU is the open-circuit voltage, ΔT is the temperature difference measured by the T-type thermocouples, d_1 and d_2 are the distances between two electrodes and two thermocouples adhered to the back of the quartz slide (near the electrodes), respectively. To obtain more precise ionic thermopower of MiTCs, multiple open-circuit voltages under different temperature differences are fitted to eliminate experimental errors.

The ionic conductivity of the MiTCs cannot be determined by the electrochemical ac impedance spectroscopy (EIS) due to the extremely low electrolyte solution. As reported by previously literatures[2, 3], the ionic thermoelectric performance of MiTCs was mainly restricted by the slow electrochemical electrode kinetics and mass transfer process of the cold electrode. The mass transfer resistance was commonly important for the characterization in ionic thermocell properties, which its accurate evaluation cannot be straightforward. The effective ionic conductivity (σ_{eff}) of MiTCs obtained from the slope of the current-voltage curve can represent the total resistance near equilibrium by using external resistance method. It can to some degree indicate the mass transfer process. The ionic conductivity of bulk redox electrolyte solution was also measured by ionic conductivity meter as controls. The $P_{max}/\Delta T^2$ of MiTCs can be obtained by connecting external resistors with different resistance values. All the experiments were repeated many times to reduce the experimental errors.

Notes S1: Fundamentals of the conventional ionic thermocells

The schematic diagram of fundamentals of the conventional ionic thermocells is shown in Scheme S4. A conventional ionic thermocell mainly consists of two electrodes and redox electrolyte. Based on the thermogalvanic effect of redox electrolytes such as $Fe(CN)_6^{4-}/Fe(CN)_6^{3-}$, Fe^{3+}/Fe^{2+}, I^-/I_3^-, etc. [4], it can continuously output electric power through continuous quasi-reversible reaction of redox ions at electrodes under temperature difference, in which the electrodes do not participate in the reaction and only transfer electrons. With the presence of temperature difference between two electrodes, $Fe(CN)_6^{3-}$ is reduced as $Fe(CN)_6^{4-}$ at the cold end, while $Fe(CN)_6^{4-}$ is correspondingly oxidized $Fe(CN)_6^{3-}$ at the hot end. Meanwhile, these product of oxidation and reduction reactions will be transferred between two electrodes by means of natural convection, concentration diffusion or thermodiffusion, and electromigration as the reactions progresses[5, 6]. When the temperature difference is presented, it would maintain the continuous generation of electric power.

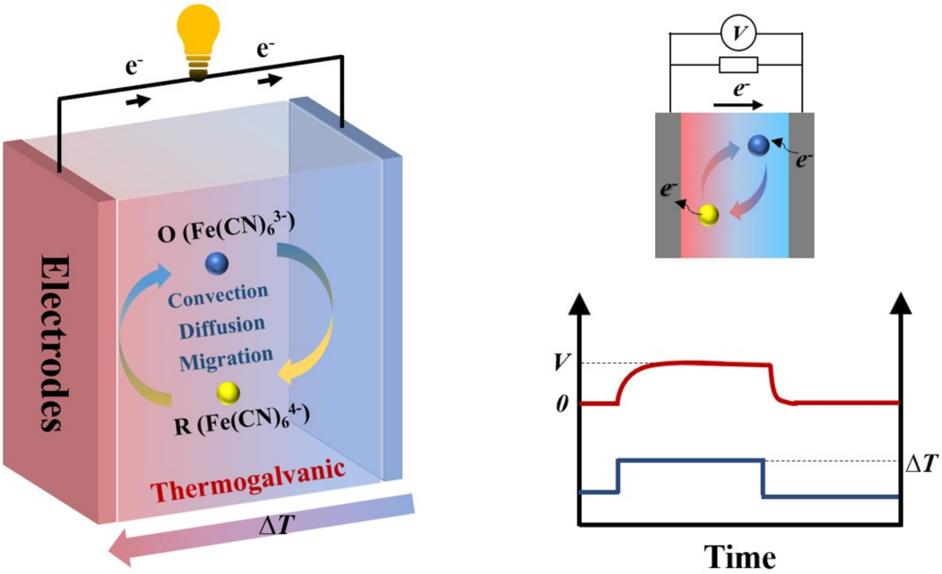

Scheme S4 Schematic diagram of the fundamentals of a typical ionic thermocell.

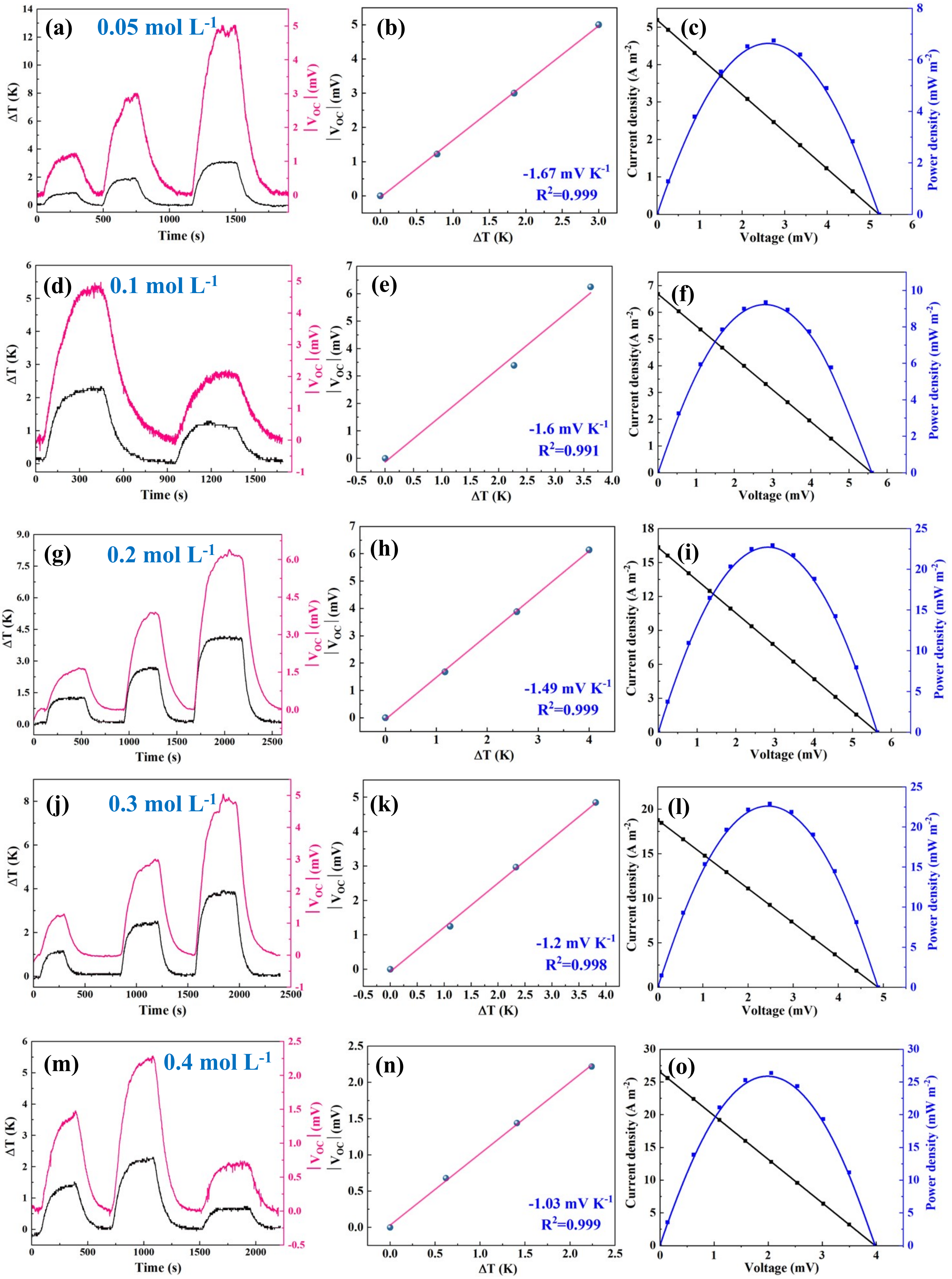

Fig. S1 Open-circuit voltage profiles and determination of the S_i as well as U-I curves (3.5 K temperature difference) with different concentration in MiTCs: (a-c) 0.05 mol L^{-1}; (b-f) 0.1 mol L^{-1};

(g-i) 0.2 mol L^{-1}; (j-l) 0.3 mol L^{-1}; (m-o) 0.4 mol L^{-1}.

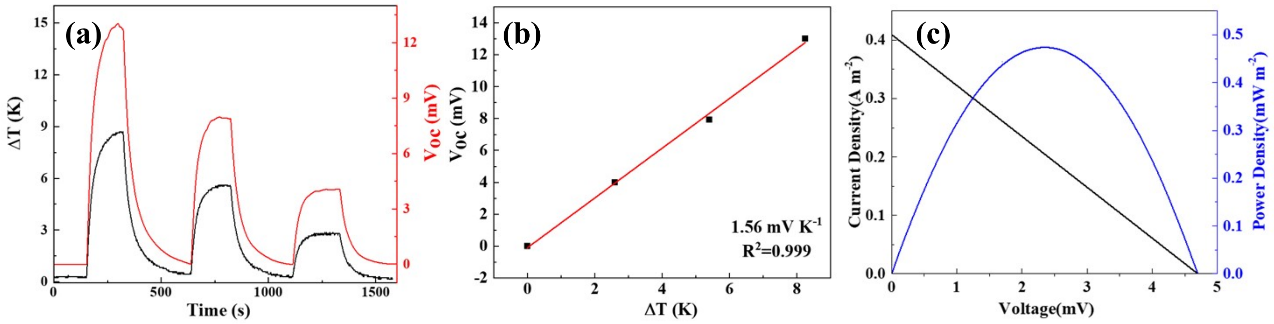

Fig. S2 Open-circuit voltage profiles and determination of the S_i as well as *U-I* curves with 0.05 mol L^{-1} concentration in LITCs.

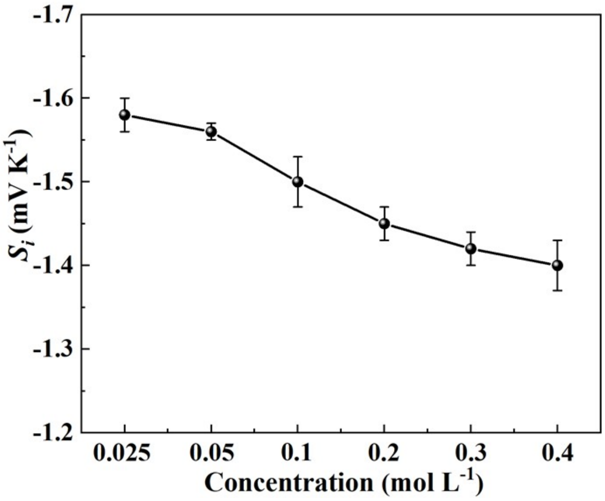

Fig. S3 Variation in the S_i of the $K_4Fe(CN)_6/K_3Fe(CN)_6$ electrolytes with different concentrations in LITCs. Error bars represent the standard deviation of more 3 repeated measurements.

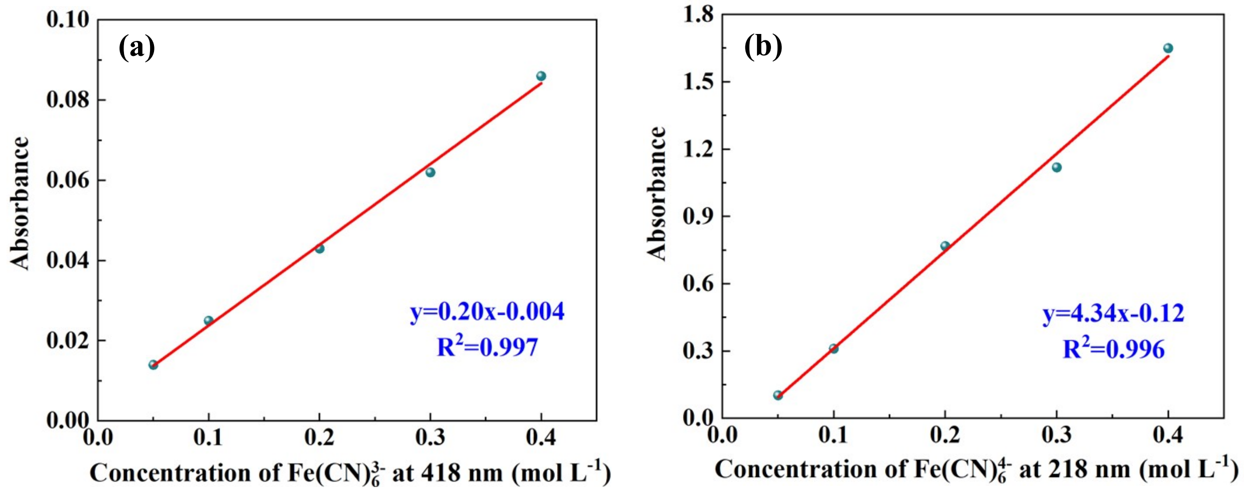

Fig. S4 (a-b) Fitting calibration curves for $Fe(CN)_6^{4-}$ and $Fe(CN)_6^{3-}$ with different concentrations from UV-vis spectra, respectively.

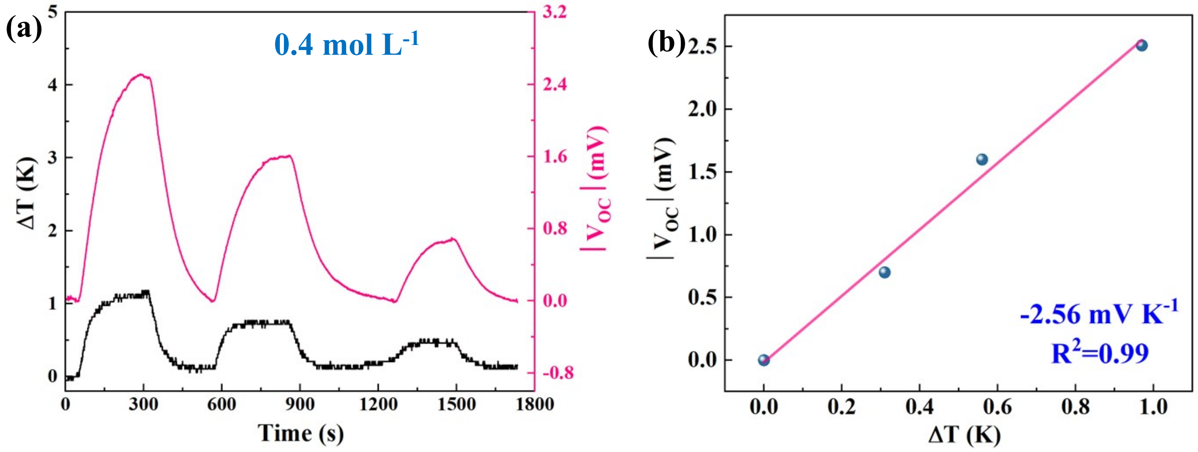

Fig. S5 Open-circuit voltage profiles and determination of the S_i for the MiTCs with positive charges.

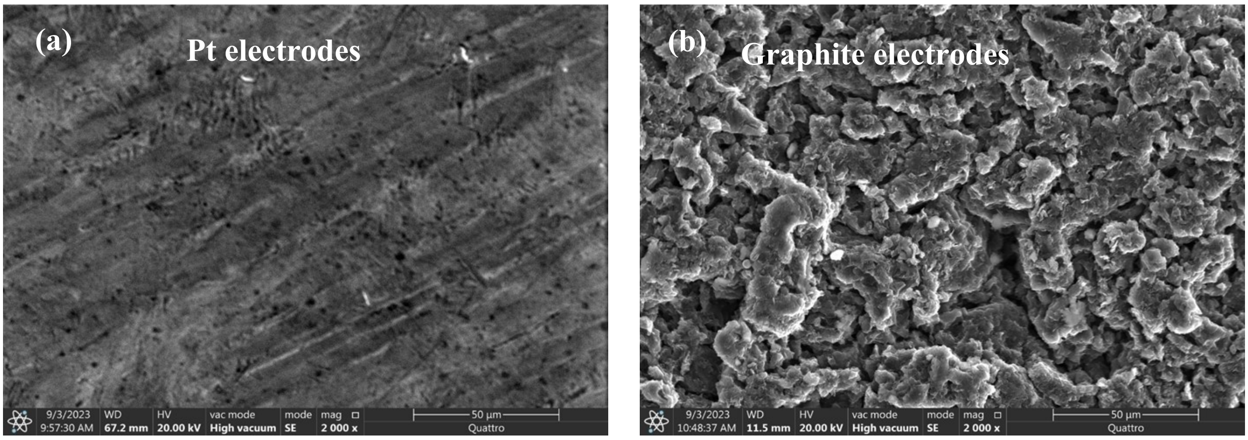

Fig. S6 Morphology of the Pt and graphite electrodes used in experiments during SEM-EDS.

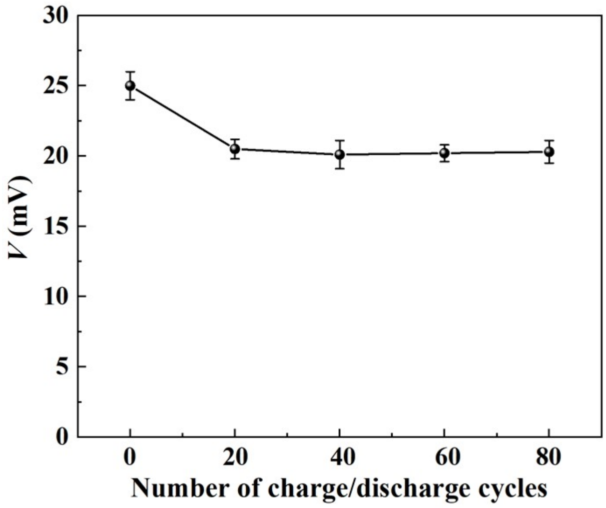

Fig. S7 Variation in the voltage when a MiTC with 0.4 mol L^{-1} electrolyte charged a 4.7 F capacitor at the temperature difference of 10 K with different numbers of charge/discharge cycles.

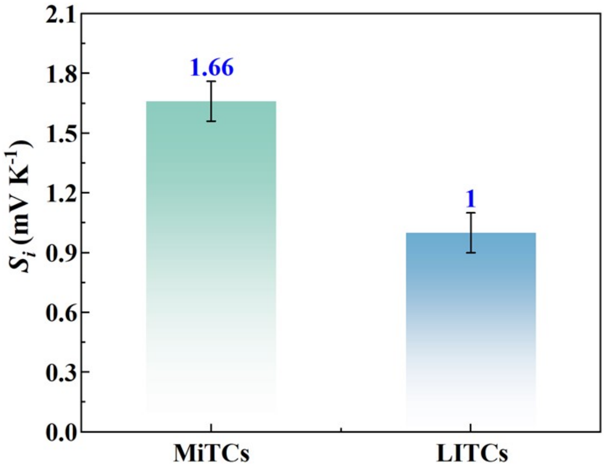

Fig. S8 Comparison of the S_i of Fe^{3+}/Fe^{2+} for MiTCs and LITCs.

Table S1 Comparison of the cross-section area, S_i and $P_{max}/(\Delta T^2)$ values of liquid-ionic thermocells. The $P_{max}/(\Delta T^2)$ values were obtained from literature reports or calculated based on the given parameters.

Redox couples	**Cross-section area (cm^2)**	**S_i (mV K^{-1})**	**$P_{max}/(\Delta T^2)$**	**Scalability**	**Ref.**
$Fe(CN)_6^{4-}/Fe(CN)_6^{3-}$	**0.001**	**-2.5**	**15.4**	**High**	**This work**
Cu/Cu^{2+}	2	-1.66	0.7	Low	[7, 8]
$Fe(CN)_6^{4-}/Fe(CN)_6^{3-}$	2.6	-3.73	7.08	Low	[2]
I^-/I^{3-}	2	+1.2	0.296	Low	[9]
$Fe(CN)_6^{4-}/Fe(CN)_6^{3-}$ (Hydrogel)	3	-9.62	0.36	Low	[10]
$Fe(CN)_6^{4-}/Fe(CN)_6^{3-}$	1	-2.9	0.64	Low	[11]
$Fe(CN)_6^{4-}/Fe(CN)_6^{3-}$ (Hydrogel)	3.14	-8.2	8.5	Low	[12]
$Fe(CN)_6^{4-}/Fe(CN)_6^{3-}$	1	-1.4	2.54	Low	[13]
$Fe(CN)_6^{4-}/Fe(CN)_6^{3-}$	2.5	-4.2	1.1	Low	[14]

References

1. G. Qian, X. Yu, Z. Li, J. Wu, R. Huang and Y. Lu, *Energy Conversion and Management*, 2020, **217**, 113005.
2. B. Yu, J. Duan, H. Cong, W. Xie, R. Liu, X. Zhuang, H. Wang, B. Qi, M. Xu, L. Wang Zhong and J. Zhou, *Science*, 2020, **370**, 342-346.
3. T. J. Kang, S. Fang, M. E. Kozlov, C. S. Haines, N. Li, Y. H. Kim, Y. Chen and R. H. Baughman, *Advanced Functional Materials*, 2012, **22**, 477-489.
4. W. Liu, X. Qian, C.-G. Han, Q. Li and G. Chen, *Applied Physics Letters*, 2021, **118**, 020501.
5. X. Qian, Z. Ma, Q. Huang, H. Jiang and R. Yang, *ACS Energy Letters*, 2024, DOI: 10.1021/acsenergylett.3c02448, 679-706.
6. W. Yang, L. Sun, J. Bao, Z. Mo, M. Du, Y. Xu and J. Zhang, *Industrial & Engineering Chemistry Research*, 2023, **62**, 12345-12355.
7. J. H. Kim, J. H. Lee, R. R. Palem, M.-S. Suh, H. H. Lee and T. J. Kang, *Scientific Reports*, 2019, **9**, 8706.
8. B. Yu, H. Xiao, Y. Zeng, S. Liu, D. Wu, P. Liu, J. Guo, W. Xie, J. Duan and J. Zhou, *Nano Energy*, 2022, **93**, 106795.
9. H. Wang, X. Zhuang, W. Xie, H. Jin, R. Liu, B. Yu, J. Duan, L. Huang and J. Zhou, *Cell Reports Physical Science*, 2022, **3**, 100737.
10. Y. Han, J. Zhang, R. Hu and D. Xu, *Science Advances*, 2022, **8**, eabl5318.
11. T. Kim, J. S. Lee, G. Lee, H. Yoon, J. Yoon, T. J. Kang and Y. H. Kim, *Nano Energy*, 2017, **31**, 160-167.
12. Y. Wang, Y. Zhang, X. Xin, J. Yang, M. Wang, R. Wang, P. Guo, W. Huang, A. J. Sobrido, B. Wei and X. Li, *Science*, 2023, **381**, 291-296.
13. H. Im, T. Kim, H. Song, J. Choi, J. S. Park, R. Ovalle-Robles, H. D. Yang, K. D. Kihm, R. H. Baughman, H. H. Lee, T. J. Kang and Y. H. Kim, *Nature Communications*, 2016, **7**, 10600.
14. J. Duan, G. Feng, B. Yu, J. Li, M. Chen, P. Yang, J. Feng, K. Liu and J. Zhou, *Nature Communications*, 2018, **9**, 5146.